NAME [redacted]

DATE 4/30/13

A library which borrows this thesis/dissertation for use by its patrons is expected to secure the signature of each user.

This thesis/dissertation by DANIEL AMBUEHL has been used by the following persons, whose signatures attest their acceptance of the above restrictions.

NAME AND ADDRESS	DATE

UNIVERSITY OF OKLAHOMA

GRADUATE COLLEGE

THE EFFECT OF CO_2 INFUSED ICE ON THE FORMATION AND DISSOCIATION OF CO_2 HYDRATE

A THESIS

SUBMITTED TO THE GRADUATE FACULTY

in partial fulfillment of the requirements for the

Degree of

MASTER OF SCIENCE

By

DANIEL AMBUEHL
Norman, Oklahoma
2013

THE EFFECT OF CO_2 INFUSED ICE ON THE FORMATION AND DISSOCIATION OF CO_2 HYDRATE

A THESIS APPROVED FOR THE
CONOCOPHILLIPS SCHOOL OF GEOLOGY AND GEOPHYSICS

BY

[redacted]

Dr. Megan Elwood Madden, Chair

[redacted]

Dr. Andrew Elwood Madden

[redacted]

Dr. Claudia Rawn

Dedications

This thesis is dedicated to my family and friends who helped me through this process and many others. In particular: Alan and Linda Ambuehl, James V. and Billie Manasco, Sam R. and Marian Ambuehl and Brittany Pritchett.

Acknowledgements

This study was completed with the funding from NASA grant # NNX09AD67G.

Table of Contents

List of Tables

List of Figures

Abstract

CO_2 gas hydrates are crystalline water ice cages around a CO_2 molecule. CO_2 affects global climate change on Earth and a major atmospheric component of the Martian atmosphere. CO_2 hydrates likely have minor effects on terrestrial atmospheric CO_2 , but may be an present in large deposits on Mars. On Earth ice deposits are found in permafrost and glaciers and contain gas bubbles. These gas bubbles may have an effect on hydrate formation and dissociation rates. Such bubbles are also likely present on Mars and may significantly influence gas hydrate fluxes. In this study, CO_2 hydrate formation and dissociation rates were measured experimentally on ultrapure and CO_2 infused water ice (ice containing previously trapped CO_2 gas bubbles). Overall, increasing pressure and temperature increased hydrate formation rates. Formation and dissociation rates both increased significantly in infused ice experiments as did the overall amount of hydrate formed. The bubbles formed during freezing of the infused ice likely provided more surface area for hydrate nucleation, increasing the rate of formation. Dissociation rates were higher in infused ice compared to ultrapure ice likely due to the larger amount of hydrate formed. Investigation of CO_2 hydrate formation from infused ice in hand sample revealed distinctive hydrate and ice layers. Most of the hydrate was observed to form in the first four hours, which agrees with other experimental data. During the dissociation of the hand sample experiments, a new opaque layer was observed forming after 5-10 minutes that is possibly hydrate. This could represent hydrate formation at room temperature and pressure through remobilization and clathration of CO_2 in the ice.

Introduction

CO_2 Hydrate

Gas hydrates are water ice cages around a 'guest' gas molecules which form in areas with low temperatures and/or elevated pressures (Figure 1) (Sloan, 1998; Koh, 2002; Kuhs et al., 2006; Hester and Brewer, 2009). On Earth, CO_2 hydrate is not as common as methane hydrate, which accounts for 95% of hydrate on Earth. However, CO_2 hydrate is commonly found in permafrost deposits and on passive margins associated with other gas hydrate phases (Koh, 2002; Hester and Brewer, 2009). Due to its relatively small volume in nature,, dissociation of CO_2 hydrate likely plays a minor control on atmospheric CO_2. A better understanding of CO_2 hydrate formation and dissociation kinetics could help mitigate excess CO_2 in the Earth's atmosphere through hydrate-based sequestration strategies (Brewer et al., 2000; Goel, 2006) .

Gas hydrate stability zones (HSZ) are found in various environments with low temperatures and moderate to high pressures. On Earth, hydrates commonly form in seafloor sediments along passive and convergent margins. On passive margins, hydrate forms through the slow accumulation of gases due to organic decay and microbial activity in pore spaces of sediment (Milkov, 2005). Hydrate accumulation rates are much faster along convergent margins compared to passive margins. In these environments hydrate forms as gas advects from the subducting slab and travels up fractures to the overlying sediment within the HSZ (Milkov, 2005).

In addition to seafloor environments, hydrates are also found in permafrost and continental glaciers. Hydrate found in permafrost forms as advecting gas travels through fractures in rock and ice. These deposits are often found as subhorizontal inclusion-free veins (Dallimore and Collett, 1995). In addition, clathrates can also form within polar ice sheets. Ice cores contain air bubbles which get trapped through the densification of snow pack into firn (Lipenkov, 2000). Within the ice there is a transition zone at depth where air bubbles disappear as the gas inside is clathrated as pressure increases due to the overlying ice.

Hydrates remain stable in continental ice until heat and unloading (decreasing pressure) cause melting at the base (Miller, 1969; Shoji and Langway, 1982, Lipenkov, 2000; Kipfstuhl et al., 2001). In these cases, the gas which exits the base of the ice is not necessarily representative of the initial gas composition due to a number of possible mechanisms. Melting events in the firn ice can release some if the air trapped in bubbles, chemical fractionation or escape due to friction and heat produced during coring or diffusion of gas through the bulk ice may contribute to the discrepancy between initial gas compositions and exiting gas (Scholender et al., 1961, Bender et al., 1995; Kipfstuhl et al., 2001; Bereiter et al., 2009).

CO_2 hydrate is also a stable phase on Mars and may be present in ice caps and/or permafrost(Miller and Smythe, 1970; Chastain and Chevier, 2007; Thomas et al., 2009; Chassefiere et al., 2013). Based on polar temperature calculations from data gathered by the Mariner 6 and 7 spacecraft, Miller and Smythe (1970) proposed that CO_2 hydrate was a stable phase in these regions. In addition to polar ice, there is a planet wide permafrost layer on Mars. Feldman et al. (2004) calculated water equivalent hydrogen levels in the near surface ranging from a minimum of 2% to a maximum of 100% at the poles based on neutron data from the Mars Odyssey spacecraft. This permafrost is another potential hydrate reservoir (Chastain and Chevier, 2007; Thomas et al., 2009;

Chassefiere et al., 2013). The top of HSZ is within the top 15 m of the Martian surface at the equator and at the surface at the poles (Chevier and Chastain, 2007). The stability field extends 3-5 km at the equator and 8-13 km at the poles (Chevier and Chastain, 2007; Thomas et al., 2009).

Hydrate formation and dissociation is also a control on atmospheric greenhouse gases, such as CH_4 and CO_2. CO_2 is a greenhouse gases which is currently contributing to climate change on Earth and could have lingering effects on a geologic timescale (Lashof and Ajuha, 1990; Archer, 2005; Cramer et al., 2006).However, natural processes will take a thousands of years to reach equilibrium with current atmospheric CO_2 concentrations. CO2 sequestration through human-initiated hydrate formation could mitigate these effects (Brewer et al., 2000; Goel, 2006). CO_2 hydrates may also sequester CO_2 on Mars, providing a major hidden reservoir of gases required for warm wet conditions early in Mars history (Hoffman, 2000; Chassefiere et al., 2013).

Understanding how hydrate decomposes can aid in modeling of the release of CO_2 from hydrate reservoirs in response to seasonal temperature fluctuations, seismic events, landslides, pore water salinity changes, impacts and changes in obliquity (Liu and Flemings, 1990; Mienert et al., 2005; Chastain and Chevier, 2007; Root and Elwood Madden 2012). A better understanding how hydrates form could also lead to a way to mechanisms to sequester CO_2 for prolonged period of time. This could potentially remove CO_2 from the atmosphere on Earth and decrease the contribution of CO_2 to climate change (Brewer et al., 2000; Goel, 2006).

The thermodynamics of CO_2 hydrate are fairly well constrained (Fuller et al., 2006; Svandel et al., 2006; Tegze et al., 2006). However, the kinetics of CO_2 hydrate formation and dissociation below the freezing point of water has received significantly less study. This has led to a lack of quantitative kinetic data required for meaningful models of CO_2 release and sequestration. Most hydrate kinetic studies have focus on methane hydrate due its prevalence and energy implications on Earth, leading to a relative lack of CO_2 hydrate kinetic data.

Gas Hydrate Formation

Wang et al. (2002) investigated the kinetics of methane hydrate formation on deuterated ice grains. They synthesized methane hydrate from crushed deuterated ice less than 250-μm in diameter over a range of temperatures of 253-273 K and studied hydrate growth through neutron diffraction. Their model suggests methane hydrate forms in three stages: initial reaction of gas with the ice surface forms a hydrate layer, growth of and diffusion through the hydrate layer to unreacted ice, and reaction of the ice core. Kuhs et al. (2006) performed a similar study and also concluded that three rate constants governed hydrate formation similar to those described b Wang et al. (2002).

Gainey and Elwood Madden (2012) measured formation and dissociation rates of methane hydrate over a range of pressures (1.7 – 3.4 MPa and 0.1 – 2 MPa, respectively) and temperatures (222 – 260 K). The experiments monitored the change in methane in headspace over time after injecting pressurized gas into a reactor containing pure water ice. Leeman and Elwood Madden (2010) used the same experimental setup but measured formation and dissociation rates for carbon dioxide hydrates. The experimental pressures were 0.75 – 0.90 MPa for formation and 0.1 and 0.45 MPa for dissociation, and temperatures 250 – 260 K. Both studies found that formation rates increase with decreasing temperature and increasing pressure, while dissociation rates increased with increasing temperatures and decreasing pressures.

From these experiments, Gainey and Elwood Madden (2012) developed a hydrate growth model within the reactor (Figure 2). They concluded that a hydrate film forms at the ice-gas contact. The gas must then diffuse through this hydrate layer to react with underlying ice and form additional hydrate. Kawamura et al. (2002) monitored hydrate formation through Raman spectroscopy and Takeya et al. (2000a) studied hydrate formation through X-ray diffraction. Both studies support the two stage model of hydrate formation.

While the two stage model of hydrate formation is generally accepted, other factors affecting clathration are not as clearly understood. For instance, there is a memory effect in gas hydrate formation. Water that has been frozen or has formed hydrate will form hydrate more readily a second time (Takeya et al., 2000b; Ohmura et al., 2003), increase the subsequent rate of formation. The mechanism for this effect is still unknown. Takeya et al. (2000b) studied CO_2 hydrate nucleation rates in CO_2 saturated liquid water. They found that nucleation rates increased by a full order of magnitude using water from melted ice compared to water which had not been previously frozen. Nucleation rates also increased with the amount of O_2 dissolved in the water. The workers attributed the increase in nucleation rate to the presence of metastable polyhedral water cages surrounding O_2 molecules formed as ice melts. These polyhedra may serve as nucleation sites upon refreezing (Takeya et al., 2000b).

Ohmura et al. (2003) also studied the effects of thermal history on hydrate nucleation rates. The workers used a hydrochlorofluorocarbon (CH_3CCl_2F) and water system. They noted that induction times were very scattered in water with previous hydrate formation and dissociation, indicating a stochastic process (Ohmura et al., 2003). Both studies found a decrease in the memory effect with heating the melted water (Takeya et al., 2000b; Ohmura et al., 2003).

Gas Hydrate Dissociation

Gainey and Elwood Madden (2012) also investigated methane hydrate dissociation rates. After formation experiments, the reactor was depressurized or warmed in order to dissociate the hydrate. The increase in gas pressure in the headspace was monitored to establish dissociation rates. Methane hydrate dissociation was found to also take place in two stages similar to formation. Initially, hydrate dissociates from the hydrate-atmosphere boundary. Overtime, an ice shell forms and further dissociation is controlled by the diffusion of gas through the ice shell.

Other studies have suggested similar mechanisms for hydrate dissociation (Stern et al., 2003; Kuhs et al., 2004; Falenty and Kuhs, 2009). These studies also noted an anomalous self-preservation quality of gas hydrate. Over the temperature range from 240 to 273 K, hydrate dissociation rates outside their thermodynamic stability are slower than expected indicating that some process is inhibiting gas diffusion. Through *in situ* neutron diffraction, Kuhs et al. (2004) determined that annealing of fractures in the secondary ice formed during initial dissociation forms an efficient barrier to diffusion over this temperature range. Falenty and Kuhs (2009) found that initial ice microstructure formed upon initial freezing also factored into the self-preservation, due to changes in the permeability of the ice. From 240 – 273 K, the ice formed upon initial dissociation has a hexagonal crystal structure, which pack together more efficiently than the cubic ice that forms at lower temperatures (Falenty and Kuhs, 2009).

Circone et al. (2003) compared dissociation behavior of CO_2 hydrate to CH_4 hydrate during isobaric temperature ramping and isothermal depressurization experiments. CO_2 hydrate released only 3% of its gas 22 K (240 K) above the hydrate phase boundary (218 K at 0.1 MPa) in contrast to the >95% gas release by CH_4 hydrate within 25 K of its phase boundary (193 K at 0.1 MPa). Only 20% of the CO_2 was released by 270 K and the system temperature was buffered at 271 K until hydrate dissociation was complete.

These microscale formation and dissociation processes may be even more important in natural heterogeneous systems where ice is not initially pure, but likely contains preexisting volatiles as bubbles or dissolved constituents. On Earth these volatiles can be found in gas bubbles in polar ice and permafrost (Miller, 1969; Shoji and Langway, 1982; Dallimore and Collett, 1995; Lipenkov, 2000; Kipfstuhl et al., 2001; Calmels and Allard, 2004). In polar ice, where ice is formed through the densification of snow pack, gas bubbles get trapped and can form up to 10% of the firn volume (Lipenkov, 2000). Bubbles are also present in permafrost deposits where they form as gas is exsolved from ground water as it freezes. The gas bubble concentration is 2% on average (Calmels and Allard, 2004). Bubbles can also be found in lake ice where they again form exsolved gas (Jefferies et al., 1994). These processes likely take place on Mars as well. Since ice on Mars can be found within continental glaciers at the poles and in a planet wide permafrost layer, gas bubbles are likely to be present. Based on the Martian atmosphere, these gas bubbles will be primarily CO_2 (Owen et al., 1977).

This study aims to establish a comprehensive dataset of CO_2 hydrate formation and dissociation rates on ultrapure water ice over a range of temperatures (245 – 260 K) and pressures (0.6 – 1.4 MPa). Once this database was established, a second dataset of CO_2 hydrate formation and dissociation rates on CO_2 infused ice was determined. These datasets were then compared to assess the effect of initial volatile content on CO_2 hydrate formation/dissociation rates. In natural systems where CO_2 hydrate is present, ice likely contains volatiles before clathration. These volatiles will vary depending on the atmospheric composition. On Earth, ice will contain mostly nitrogen and oxygen while on Mars the primary volatile will be carbon dioxide. These volatiles could affect hydrate formation and dissociation in ice cores on Earth, ice caps on Mars, and frozen lakes or oceans preserved as permafrost on both.

Methods

The single hydrate reactor (1HR) experimental apparatus is comprised of a gas tank, reserve vessel, and reactor with connecting valves and an exit line (Figure 3A). A second experimental apparatus – the triple hydrate reactor (3HR) – was developed in order to accelerate the data collection process. The second apparatus consists of a reserve tank attached to three reactors (Figure 3B). Table 1 contains important dimensions for 1HR and 3HR.

CO_2 infusion of ice

The each reactor was pressurized to approximately 0.34 MPa with research grade CO_2 and left for 14-16 hours at room temperature. This pressure was selected because it was outside the hydrate stability field over the range of experimental temperatures. Pressure and temperature measurements were taken every 30 seconds to record the pressure decrease, which was attributed to loss of gas from the headspace through diffusion of the gas into the water. Saturation was approached when no more loss of headspace gas was measured. The reactor with the gas-saturated water was then frozen in a commercial freezer to temperatures between 245 and 260 K. Since gas molecules were excluded as the water froze, the pressure was recorded again to determine the amount of gas released from the freezing water to the headspace. Pressure and temperature were recorded every 30 seconds over 21-24 hours, with the increase in reactor pressure attributed to the exclusion of gas from the water ice as well as expansion of the water as it froze. The number of moles of gas diffused into the water and portion excluded from ice were calculated using the van der Waals equation (Equation 2), where P is the pressure (Pa), V is the volume (m^3), n is the number of moles (mol), R is the universal gas constant (8.314 Pa m^3 mol^{-1} K^{-1}), T is the temperature (K), a is a constant (m^6Pa mol^{-2}) and b is a constant ($m^3 mol^{-1}$). For CO_2, a = 0.364 m^6Pa mol^{-2} and b =$4.267x10^{-5}$ $m^3 mol^{-1}$.

$$(P + \frac{n^2a}{V^2})(V - nb) = nRT \qquad \text{(Equation 1)}$$

Formation/Dissociation

Hydrate formation experiments were performed at conditions similar to those described in Gainey and Elwood Madden (2012) and Leeman and Elwood Madden (2010). To perform a hydrate formation experiment using UP or CO_2 infused ice, the freezer was set to the experimental temperature between 245 and 260 K. The selected gas was put into the reserve tank and allowed to cool to experimental temperature. From the reserve tank, the gas was let into the reactor(s) at a pre-set pressure between 0.6 and 1.4 MPa. For formation experiments, headspace pressure and reactor temperature readings were gathered over 4-10 hours at 15 second intervals.

In order to dissociate the hydrate, the reactor was depressurized to a predetermined pressure between 0.1 and 0.5 MPa and resealed. Temperature was kept constant for coupled formation/dissociation experiments between 245 and 260 K. The dissociation experiments ran for 4-10 hours until the headspace pressure plateaued.

Data Collection

Data was collected using Labview/National Instruments software. The software recorded the time (seconds), pressure (psi), and temperature (℃) of the reactor(s). During formation/dissociation experiments data were recorded every 15 seconds. Data were recorded every 30 seconds during the longer gas saturation/ice exclusion experiments.

Data processing and rate determination

The data was processed by inserting the time, reactor temperature and reactor pressure into a macro-enabled Excel spreadsheet. The spreadsheet converted the pressure to from pounds per square to Pascals and the temperature from Celsius to Kelvin. These measurements were then used in the van der Waal's equation (Equation 1) to calculate the number of moles of gas in the reactor headspace at each data point. The number of moles of gas in the headspace was then plotted versus the time. A third order polynomial trendline was fit to the curve generated. The initial rate of formation or dissociation was determined by taking the derivative of the equation and setting time equal to zero. The initial rate was then divided by the surface area for normalization. The surface area for each apparatus is found in Table 1.

Visual observations of CO_2 infused ice and clathrated ice

In order to examine how the hydrate grew in the reactor, a known volume of water was placed in a separate reactor system (Figure 4). The procedure for infusing the ice described above was followed. After infusing, the ice was taken out of the container and observed. After observing the infused ice in hand sample the experiment was repeated with hydrate formation immediately following infusion. Hydrate was allowed to form for set periods of time and then taken out of the reactor and observed. Observations were made at 60 minutes, 2 hours, 4 hours and 8 hours. The smaller time intervals were chosen to investigate the period where hydrate formation is the most rapid.

Results and Discussion

CO_2 infusion

After injecting CO_2 into the reactor(s) and a steady decrease of headspace pressure was observed (Figure 5). This decrease is interpreted as diffusion of CO_2 into the water. Over time (approximately 35,000 seconds on Figure 5) the curve begins to flatten, indicating the water is approaching saturation. The average amount of CO_2 diffused into the water for 1HR and 3HR was 0.086 and 0.076 mol/L, respectively (Table 2).

Freezing of the infused water takes place in multiple stages (Figure 6). Between zero and 20,000 seconds, the pressure inside the reactor decreased partially due to decreasing temperature and partially due to further diffusion of CO_2, due to the increase in CO_2 solubility as water temperature decreases (Wiebe and Gaddy, 1940). After the initial crystallization of ice (approximately 20,000 seconds on Figure 6) the temperature sharply increases. This increase is due to the undercooling of liquid water to crystallize ice. Once the first ice forms, the temperature of the system is buffered back to ~273 K. There is a second, smaller increase (approximately 35,000 seconds on Figure 6), which is likely caused by the latent heat released from crystallization of the last liquid water. The average amount of CO_2 excluded from the water during freezing for 1HR and 3HR was 0.0591 and 0.0293 mol/L, respectively (Table 2).

The overall concentration of CO_2 in the infused ice for the 1HR set up averaged 0.0269 mol/kg and 0.0467 mol/kg for 3HR (Table 2). The difference in concentration may be attributed to surface area and how the water freezes in the different reactor vessels (Table 1). The 1HR set up has nearly four times the surface area as the 3HR. Therefore it may take longer to form the ice cap in the 1HR system, allowing more CO_2 to escape before freezing is complete.

Infused Ice

Following the infusion process the ice is banded in the top 1.5 – 2.5 cm. The bands alternate between thicker, opaque, bubble filled ice and thinner, transparent, relatively bubble free ice (Figure 7). The ice below the banding is a semitransparent, cloudy massive layer of ice. Though this bottom layer has bubbles, the bubble concentration is much lower than in the opaque banded layers. This banding effect is likely caused by minor temperature cycling within the freezer. The freezer cools to the set temperature and then switches off. The motor only switches on again when the freezer temperature has warmed a certain amount above the set point. During the cooling period the white, cloudy layers form because more gas is exsolved from the water as it freezes (Figure 8). The clear ice layers form as the freezer warms and less gas is exsolved because freezing does not occur as quickly. This is similar to banding seen in lake ice due to diurnal temperature variation (Jefferies et al, 1994). The lack of banding at the bottom is most likely due to the manner in which the water freezes. Unlike a lake where water freezes from the top down due to colder atmospheric temperatures, the water in the reactor is surrounded by freezing temperatures. The water in the reactor freezes from the sides, in addition to the top. This process causes the entire beaker to exsolve CO_2 concentrating it at the top. The remaining CO_2 is incorporated in the massive cloudy layer. Martian ice formed through the freezing of surface water could exhibit the same type of banding. Gas bubbles in terrestrial ice contain atmospheric gas compositions, containing mostly nitrogen and oxygen, while on Mars the composition would likely be 95% CO_2 (Owen et al., 1977).

Formation

In all formation experiments, hydrate formation is inferred from the decrease in pressure in the headspace over time (Figure 9). The rate of formation is initially rapid, but slows as the experiment proceeded. The decrease in rate could be caused by a change in the rate limiting process. The initial, rapid formation is likely controlled by the amount of ice surface area with which the gas can react. As hydrate is formed, the available surface area decreases and a hydrate film is formed. Further hydrate formation is likely controlled by diffusion through this film (Wang et al., 2002; Kuhs et al. 2006, Gainey and Elwood Madden, 2012).

Our results show an increase in formation rate with increasing pressure and increasing temperature. The formation rates for both infused and UP ice experiments increase with increasing pressure and decreasing temperature (Figure 10). An increase in pressure provides a larger driving force and more material for clathration, while at higher temperatures more energy is available to transform ice and gas into hydrate, leading to faster rates. Similar effects have also been observed in methane hydrate formation rates (Gainey and Elwood Madden, 2012). However, infused CO_2 ice produces the most profound effect on CO_2 hydrate formation rates (Figure 11). The trapped gas bubbles increase the hydrate formation rates by approximately an order of magnitude. In addition to faster initial rates, there was also more headspace CO_2 consumed, indicating more overall hydrate was formed.

Figures 10 and 11 show a higher standard deviation in the rate of formation within the ultrapure water experiments compared to those using infused ice. This may be due to the stochastic nature of gas hydrate nucleation (Bishnoi and Natarajan, 1996). McCallum et al. (2007) conducted gas hydrate formation experiments in a 70 L and a 450 mL pressure vessels. The standard deviation of the rates measured via experiments in the larger vessel was much lower than the standard deviation of rates measured in the smaller reactor, indicating that increasing surface area decreases the contribution of outliers to the overall rate of hydrate nucleation (McCallum et al., 2007). The gas bubbles in the infused ice are likely increasing the amount of surface area available for clathration, resulting in lower standard deviations and faster rates of clathrate formation.

The amount of reacting surface area directly affects the rate of hydrate formation (Wang et al., 2002; Kuhs et al. 2006). The bubbles trapped in the infused ice experiments increase the surface area in the ice below the ice surface. As the hydrate front moves downward in the ice the bubbles not only provide additional surface area for the formation reaction, but also more CO_2 for clathration (Figure 12). The volume change between ice and hydrate is not significant (Sloan and Koh, 2008). Therefore, it is unlikely that the phase change would create microfractures and create additional surface area.

The pressures inside the CO_2 bubbles are set at their formation pressures, for these experiments ~0.34 MPa. This pressure was well below the hydrate stability field, so there is no clathration occurring in the bubbles until the headspace is pressurized into the HSF. The experimental pressures for hydrate formation experiments were not high enough to affect the bubbles trapped in the ice. The only way to clathrate the bubbles is the advance of the hydrate front from the headspace.

The shape of the hydrate formation curves on UP and infused ice are nearly identical indicating that the same processes are going on in both types of experiments (Figure 9). Both types of experiments had faster instantaneous rates of formation until approximately 12,500 seconds. This indicates that until around 12,500 seconds hydrate formation is likely controlled by surface area, but after this point diffusion becomes the rate determining process. In the later diffusion-growth stage more hydrate is formed in the infused ice experiments than in the UP ice. This is most likely due to the presence of additional gas within bubbles in the infused ice as well as increased surface area for reaction once the gas is diffused.

Dissociation

Gas hydrate dissociation is inferred from increases in headspace gas pressure after depressurizing the reactor (Figure 13). The initial rate of dissociation was very rapid but decreased as the dissociation experiment proceeded. Similar to the formation experiments, this decrease in dissociation rate may be due to a change in the rate controlling mechanism from a surface area dominated process to diffusion. The surface of the hydrate dissociates first but formation of an ice film hampers further dissociation.

The relationship between hydrate dissociation rates and pressure and temperature is more complex than observed in formation experiments. There is a temperature range from 240 to 273 K where CO_2 hydrate exhibits an anomalous 'self-preservation' (Stern et al., 2003; Kuhs et al., 2004; Falenty and Kuhs, 2009). Over this range hydrate dissociation is slower than expected. The major factors affecting hydrate dissociation are the initial microstructure of the ice, which is dependent on temperature, and the amount of annealing of fractures formed during initial dissociation (Kuhs et al., 2004; Falenty and Kuhs, 2009).This anomalous preservation behavior is visible in this study where the dissociation rates form a V-shape over the temperature range between 245 and 260K, reaching an apparent minimum around 250 K, in both UP and infused ice experiments (Figure 14). At temperatures around 250 K, ice microstructure and annealing effects make the ice more impermeable than at other temperatures (Falenty and Kuhs, 2009).

While the V-shape is visible in both UP and infused ice the rate of dissociation was faster in the infused ice experiments. This is most likely due to the larger amount of hydrate that was formed on this ice; similar results were observed in methane hydrate dissociation experiments where the concentration of hydrate strongly affected the dissociation rate (Gainey and Elwood Madden 2012). Formation experiments using infused ice at 250 K yielded less hydrate than at higher and lower temperatures. This explains the proximity of the UP and infused ice points at 250 K in Figure 14. The ice microstructure at 250 K may be more perfect, making it more impermeable to gas diffusion and therefore abundant hydrate formation.

Hand sample observations

Observations of CO_2 hydrate formation at 1, 4, and 8 hours reveal that the hydrate advanced down through the ice as time increases (Figure 15). However, most of the hydrate layer is formed within the first four hours. This time coincides with the decrease in slope seen in the formation experiments at 12,500 seconds (Figure 9A and B). This may represent the transition point where diffusion becomes the rate-limiting control on hydrate formation. The hydrate film extends to the bottom of the banding, leaving the underlying massive ice layer relatively unaltered. Hydrate also forms preferentially along the sides of the ice, rather than in the center. This is likely due to easier migration pathways between the glass beaker and ice than through the ice itself.

Observations of the infused ice also reveal the morphology at the top of the ice. The ice is not flat as expected, instead there is a convexity, or bump, to one side. This bump is possibly formed by the freezing of water with high concentrations of exsolved CO_2 bubbles (Figure 16). The cooling and freezing of the water exsolves CO_2 into the gas phase. This gas bubbles up through the water to the headspace. Once ice starts to form at the top of the water, the surface area available for the CO_2 to escape decreases. Eventually the hole through which the gas is escaping freezes over. The water frozen here contains a high abundance of gas bubbles causing the bumpy morphology. These bumps were seen in both the infused ice and UP ice, but the infused ice had more bumps. The non-flat top seen in UP ice is likely due to the expansion of ice in a confined container. Expansion of ice also contributes to the bumpy surface of the infused ice. The bubbling of the exsolved gas helps focus the volume expansion due to freezing up toward the top of the beaker. These bumps complicate rate determination since the exact surface area is unknown. The surface areas used in this study were calculated assuming a flat cross section of each reactor. With bumps present, this surface area will increase. This could cause the surface area normalized rates to appear faster than they are in reality.

Unusual texture change

Dissociation of the hand samples reveals a previously undocumented phenomenon. Initially, the beaker contains an opaque hydrate layer and an ice layer (Figure 17). As the bottom of the beaker warms, a new opaque layer forms. The texture of this layer is the same as the original hydrate. This opaque material continues to grow up along the sides of the beaker until it joins with the original hydrate layer and the boundary between the two became obscured (Figure 17). This layer is observed forming in all visual experiments as they warmed.

At this time the mechanism for hydrate formation at room temperature and atmospheric pressures is unknown. It is possible that the warming of the beaker base releases some of the CO_2 stored in bubbles into a free gas phase. This released gas travels upward and encounters colder ice above. This ice will be closer to the experimental conditions. If the CO_2 is released in sufficient quantity, this could react with the cold ice to form hydrate.

Conclusion

Carbon dioxide hydrates form faster under higher pressures and higher temperatures, similar to trends observed for methane hydrates (Gainey and Elwood Madden, 2012). Therefore, CO_2 hydrate formation at the Martian equator would likely be faster than at the poles due to the higher temperatures and higher pressures in the hydrate stability field (Root and Elwood Madden, 2012). However, the amount of overall hydrate formed is dictated by mass transport of gas. Therefore, while hydrates may form faster at the equator this does not necessarily mean that lower latitudes will have larger hydrate deposits. The overall amount of hydrate is controlled by the amount of advecting gas, which is dependent on subsurface processes. The same processes are not likely active across the entire planet, leading to localized hydrate deposits.

These results show that CO_2 hydrate formation takes place in two stages as suggested in other studies (Takeya et al., 2000a; Kawamura et al., 2002; Gainey and Elwood Madden, 2012, Falenty et al., 2013). The first stage is a rapid formation process controlled by available surface area, forming a hydrate shell at the ice-gas interface. The second stage is slower and controlled by diffusion of CO_2 through the hydrate shell to react with the underlying ice. The majority of hydrate was formed in the first four hours.

Examining the hydrate in the beakers also showed preferential growth along paths of maximum permeability. In the beakers, hydrate formed along the sides of the beaker compared to the middle. This supports the accepted model for the formation of sub horizontal hydrate veins observed by Dallimore and Collett (1995) in the Alaskan permafrost. These hydrate veins could have formed as gas moved along fractures in the ice.

Infusing water with CO_2 creates bubble-filled ice upon freezing. This provides additional surface area and CO_2 within the ice, making clathration more favorable. In natural systems, ices formed from snowfall or the freezing of lakes and oceans also contain bubbles, but do not have as high a bubble population density because natural waters are not as saturated in CO_2 or other gases. On Mars, air bubbles could have been incorporated into polar ice caps through compaction of snow. If permafrost or ice formed from standing water, similar to the water in our beaker, the gas bubbles would also exsolve from the liquid water as it froze forming bubbles. These bubbles would be comprised of at least 95% CO_2 based on the Martian atmosphere. This trapped CO_2 would be available for clathration. Our CO_2 hydrate experiments also show an anomalous self preservation effect during dissociation. Dissociation rates do not increase linearly with temperature and pressure. Instead, rates slow between 240 to 260 K, reaching a minimum around 250 K. These results reinforce the findings of other studies which noted a decrease in hydrate dissociation rate from 240 to 273 K (Stern et al., 2003; Kuhs et al., 2004; Falenty and Kuhs, 2009). Kuhs et al. (2004) attributed this to the annealing of fractures formed during initial hydrate dissociation. Building on this, Falenty and Kuhs (2009) also found a strong correlation with the microstructure and the permeability of the ice. This could enable hydrate deposits to survive conditions fluctuations above the hydrate stability field and persist after conditions return to the stability field. Temperatures near the Martian equator warm into this range, making metastable hydrate is likely at these latitudes (Kieffer et al., 1976).

Dissociation of hydrate from infused ice was significantly faster than dissociation from UP water ice. This increase is most likely caused by the increased amount of hydrate formed during experiments using the infused ice. A similar effect of hydrate concentration on dissociation rates was found by Gainey and Elwood Madden (2012) in CH_4 hydrate dissociation. On Mars, gases migrating from the subsurface will encounter permafrost or polar ice caps. Multiple reactions during the alteration of subsurface basalt create CO_2 and possibly CH_4 as by-products (Oze and Sharma, 2005). This gas then advects to the surface and may encounter bubbles trapped in permafrost , ancient ocean/lake ice, or the polar caps (Figure 18). These bubbles will likely have lower pressures and contain mostly CO_2 which will enable hydrate to grow within them. This could lead to larger hydrate deposits than would be possible in bubble-free ice. In the polar regions of Mars, these bubbles could also facilitate hydrate formation from atmospheric CO_2 during colder temperatures.

The unusual dissociation seen in the time lapse experiments could have significant implications if a new hydrate layer is being formed from gas released from the ice. This could mean that a heat source beneath an ice cap would cause gases in hydrate and free gas phase to be released and migrate upward. If these gases reach a zone far enough away from the heat source and within the hydrate stability field they could accumulate in a hydrate phase. This could lead to formation of ice layers enriched in CO_2 hydrate on Mars.

Tables

Table 1 Important properties of each experimental set up.

Reactor Name	Number of Reactors	Headspace Volume (mL)	Ice Volume (mL)	Surface Area (m^2)	Reserve Volume (mL)
1HR	1	128.4	371.6	0.006204	500
3HR	3	60 (per reactor)	90	0.00166	300

Table 2 Average values for the amount of CO_2 trapped in the infused ice for each experimental set up

Reactor name	CO_2 in liquid water (mol/L)	CO_2 excluded from ice (mol/L)	CO_2 left in ice (mol/L)	CO_2 concentration in ice (mol/kg)
1HR	0.086	0.0591	0.0269	0.0296
3HR	0.076	0.0293	0.0467	0.0467

Table 3 Formation Rates

P (MPa)	T (K)	System	Type of ice	Log rate (mol/m^2s)
0.58	246	3HR	UP	-5.07
0.58	246	3HR	UP	-5.48
0.58	246	3HR	UP	-4.87
0.69	245	3HR	UP	-4.59
0.69	245	3HR	UP	-4.61
0.69	245	3HR	UP	-4.70
0.75	250	1HR	Infused	-3.38
0.79	245	3HR	Infused	-3.88
0.79	245	3HR	Infused	-3.88
0.79	245	3HR	Infused	-3.88
0.79	247	3HR	UP	-4.46
0.79	247	3HR	UP	-4.45
0.79	247	3HR	UP	-4.33
0.79	250	3HR	UP	-4.50
0.79	250	3HR	UP	-4.57
0.89	245	3HR	UP	-4.45
0.89	245	3HR	UP	-4.37
0.89	245	3HR	UP	-4.40
0.93	257	3HR	UP	-4.25
0.93	257	3HR	UP	-4.56
0.98	260	1HR	Infused	-3.22
1.03	245	3HR	UP	-4.45
1.03	245	3HR	UP	-4.12
1.03	245	3HR	UP	-4.12
1.03	259	3HR	UP	-4.16
1.03	259	3HR	UP	-3.81
1.03	259	3HR	UP	-4.63
1.05	245	3HR	Infused	-3.39
1.05	245	3HR	Infused	-3.39
1.05	245	3HR	Infused	-3.36
1.08	260	1HR	Infused	-3.12
1.09	260	1HR	Infused	-3.06
1.14	245	3HR	UP	-4.44
1.14	257	3HR	UP	-4.15
1.14	257	3HR	UP	-4.65
1.14	257	3HR	UP	-4.09
1.41	255	3HR	UP	-4.72
1.41	255	3HR	UP	-4.26
1.41	255	3HR	UP	-4.61

Table 4 Dissociation rates

P (MPa)	T (K)	System	Type of ice	Log Rate (mol/m^2s)
0.10	244	3HR	UP	-4.95
0.10	244	3HR	UP	-4.87
0.10	244	3HR	UP	-4.85
0.10	245	3HR	UP	-4.82
0.10	245	3HR	UP	-4.95
0.10	245	3HR	UP	-4.89
0.10	245	3HR	Infused	-3.74
0.10	245	3HR	Infused	-3.39
0.10	245	3HR	Infused	-3.56
0.10	246	3HR	UP	-4.58
0.10	246	3HR	UP	-4.50
0.10	246	3HR	UP	-4.43
0.10	248	1HR	Infused	-4.21
0.10	250	3HR	UP	-4.59
0.10	250	3HR	UP	-4.49
0.10	257	3HR	UP	-4.47
0.10	257	3HR	UP	-4.42
0.10	257	3HR	UP	-4.11
0.10	257	3HR	UP	-4.62
0.10	257	3HR	UP	-4.76
0.10	259	3HR	UP	-4.29
0.10	259	3HR	UP	-4.45
0.10	259	3HR	UP	-4.42
0.10	260	1HR	Infused	-4.51
0.10	260	1HR	Infused	-3.70
0.10	260	1HR	Infused	-3.62
0.31	245	3HR	UP	-4.32
0.31	245	3HR	UP	-4.04
0.31	245	3HR	UP	-4.01
0.45	255	3HR	UP	-4.54
0.45	255	3HR	UP	-4.65
0.45	255	3HR	UP	-5.15

Figures

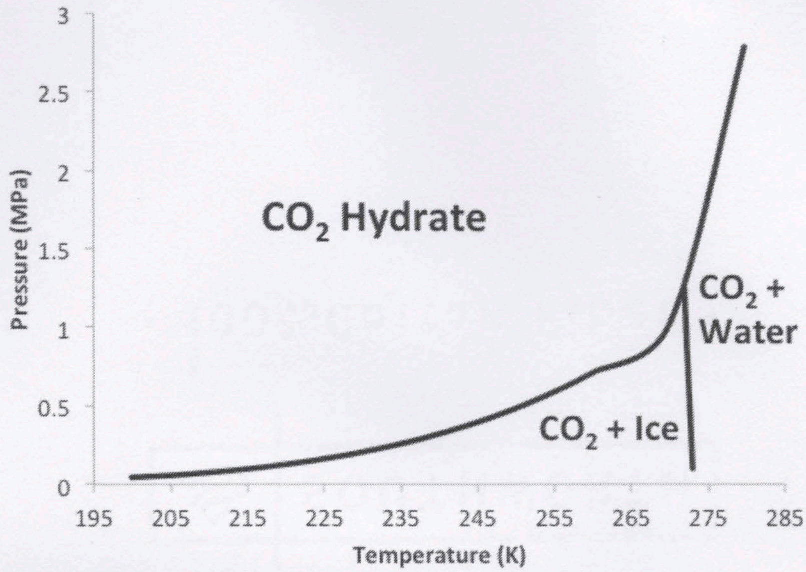

Figure 1 Phase diagram of CO_2 hydrate, as well as the ice/water boundary. Constructed using HYDOFF (Sloan and Koh, 2007).

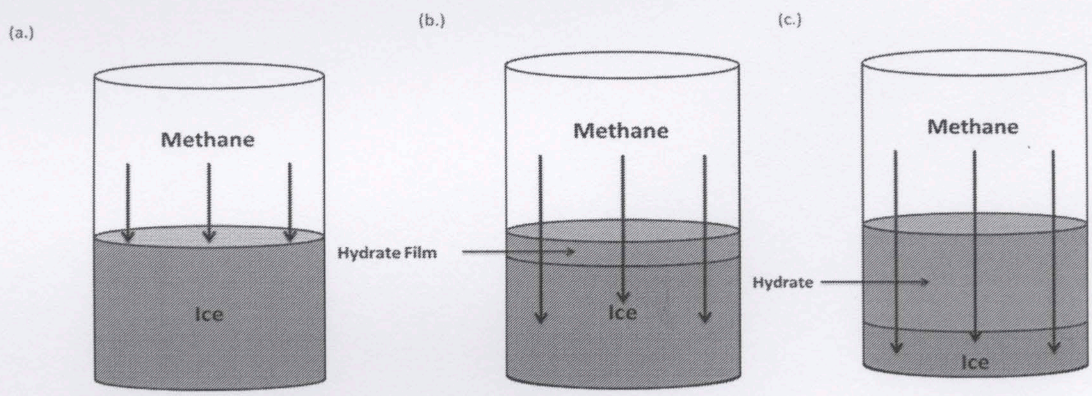

Figure 2 The model of hydrate growth developed by Gainey and Madden (2012). Gas reacts with the ice to form a hydrate layer. For further clathration, the gas must diffuse through this layer to react with more ice (Gainey and Maddden, 2012).

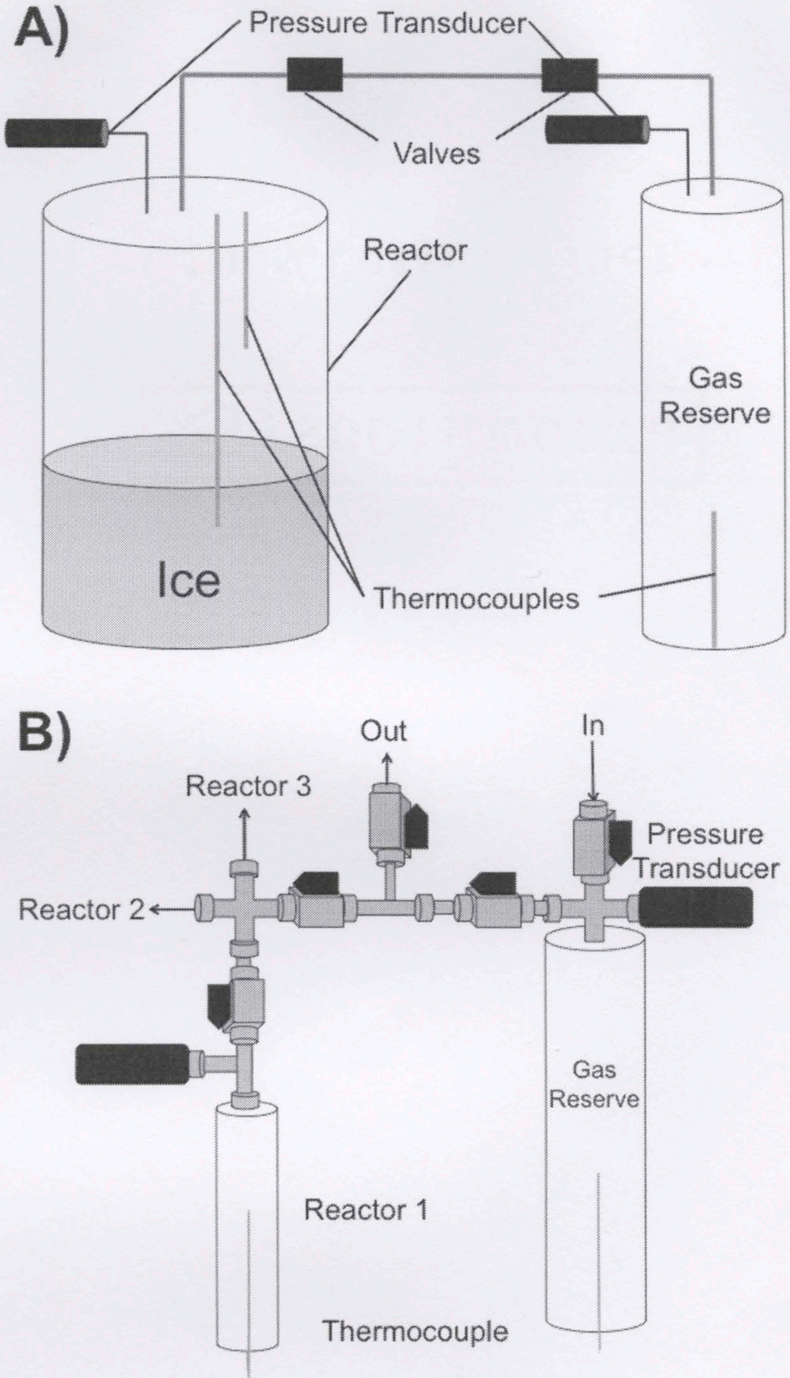

Figure 3 A) Schematic of the 1HR experimental apparatus. Gas is injected into the reserve where it cools to the experimental temperature. After cooling the gas is transferred to the reactor where it reacts with ice to form hydrate. B) Schematic of the 3HR apparatus. This apparatus follows the same method as the 1HR, but the 3HR allows for the three experiments to be completed at once under the same P-T conditions. Each reactor in the 3HR apparatus has its own pressure transducer.

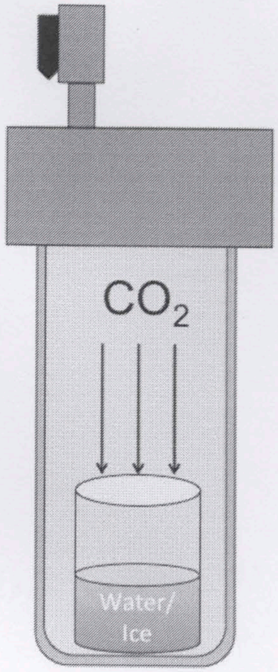

Figure 4 The infused ice/hydrate used in the visual experiments was created in a separate reactor. A 100 mL beaker was filled with 70 mL of water and infused with CO_2. After infusion, the reactor was pressurized into the HSF. The ice was inspected before clathration and at 30 minutes, 1 hour, 2 hours, 4 hours, and 8 hours.

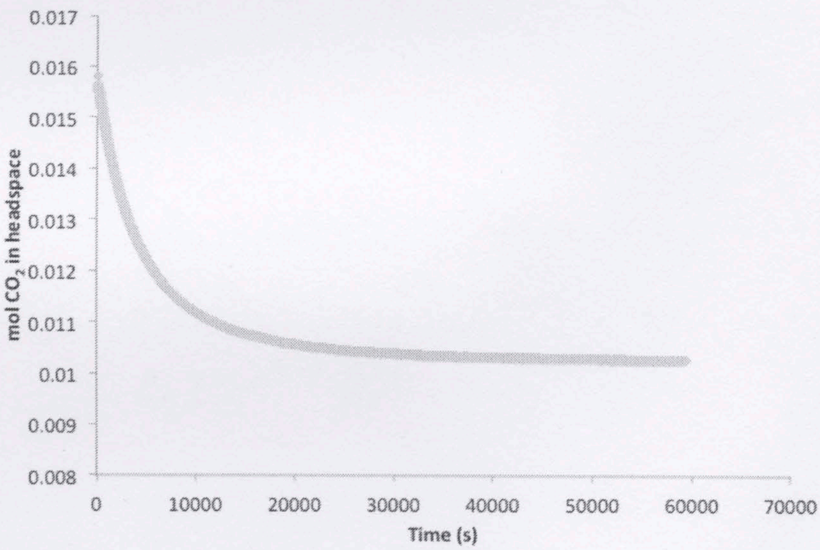

Figure 5 Diffusion of CO_2 into the water at room temperature. Flattening of the curve with time indicates that the water is approaching saturation with CO_2.

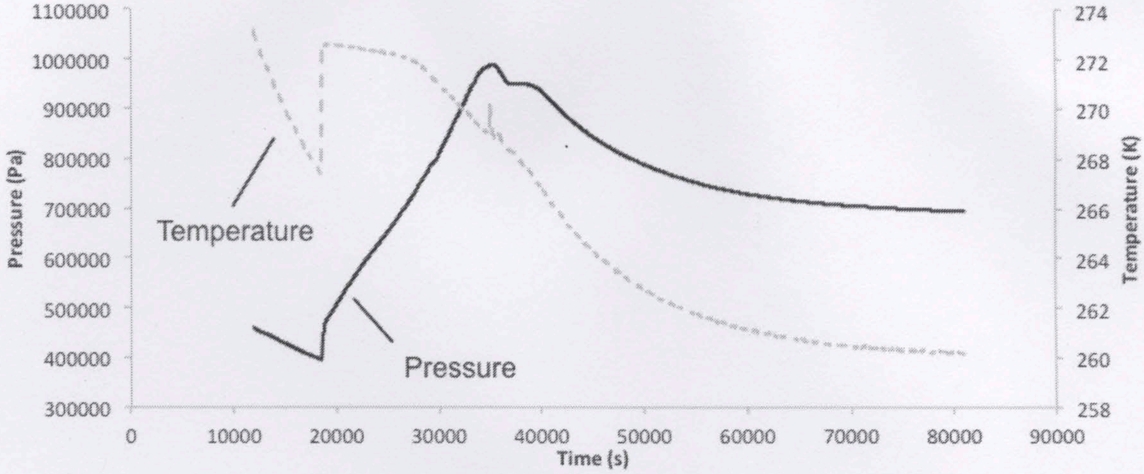

Figure 6 The temperature (gray, dashed line) and pressure (black, solid line) conditions in the reactor during the formation of CO_2-infused ice. The sharp increase in pressure and temperature (~20,000 s) is caused by the first crystallization of ice. The second smaller increase (~35,000 s) is likely caused by the freezing of the last water.

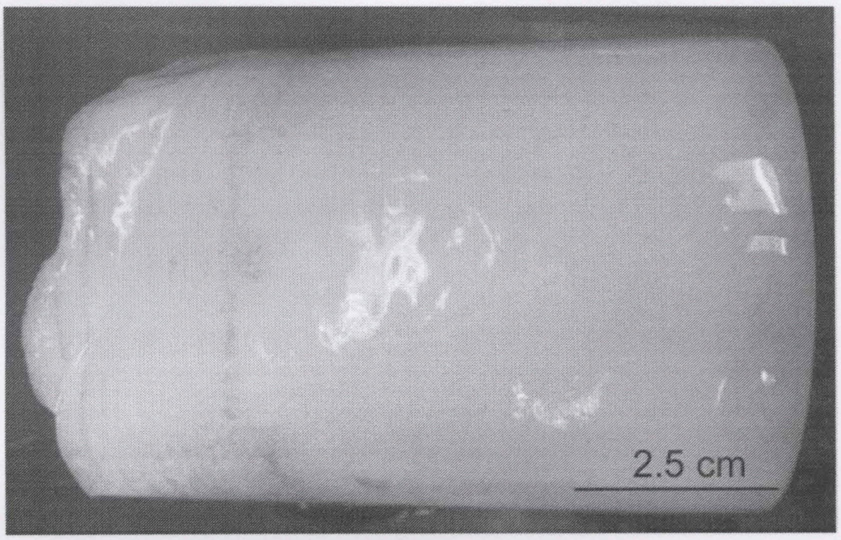

Figure 7 The infused ice was banded in the top 2.5 cm. The thickness of the banding varied between 1.5 – 2.5 cm depending on the volume of water.

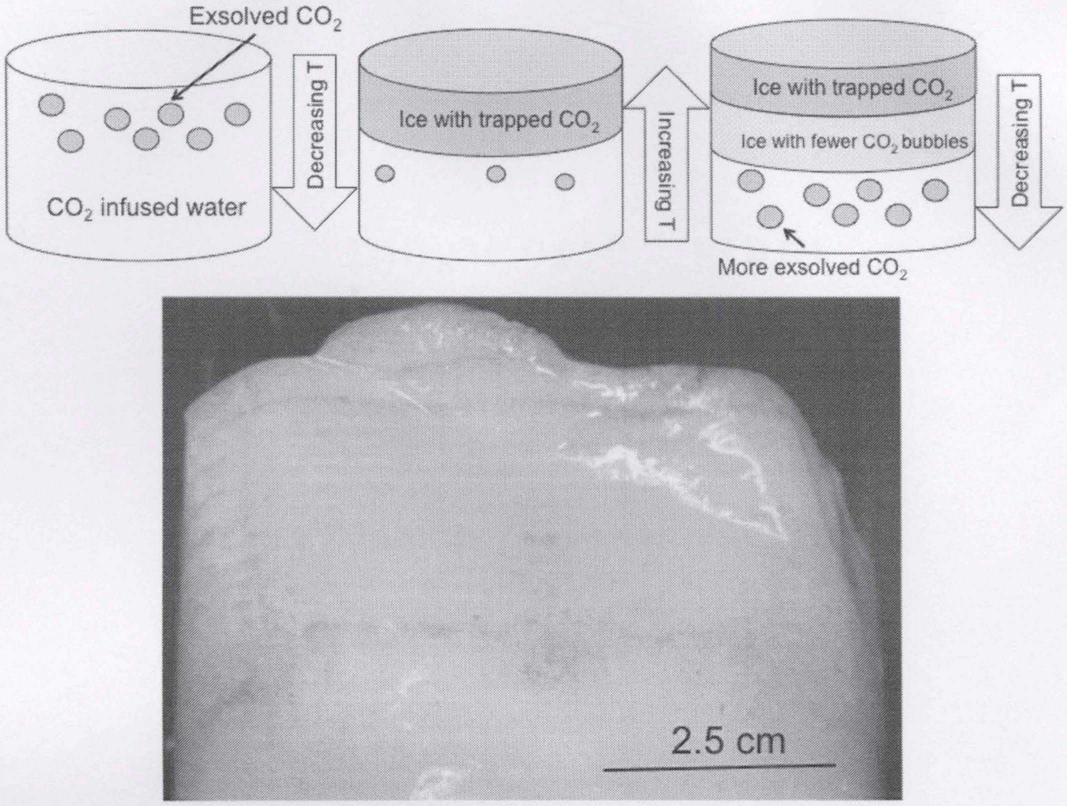

Figure 8 The formation of the banding in the CO_2 infused ice is caused by small temperature fluctuations in the freezer. As the temperature cools gas is excluded from the water this gas is stored in the opaque layers of the banding (gray layer). However, once the freezer reaches the set temperature the motor shuts off and the freezer gradually warms until the motor kicks back on. During these warming periods, less gas is excluded resulting in the thinner, transparent layers.

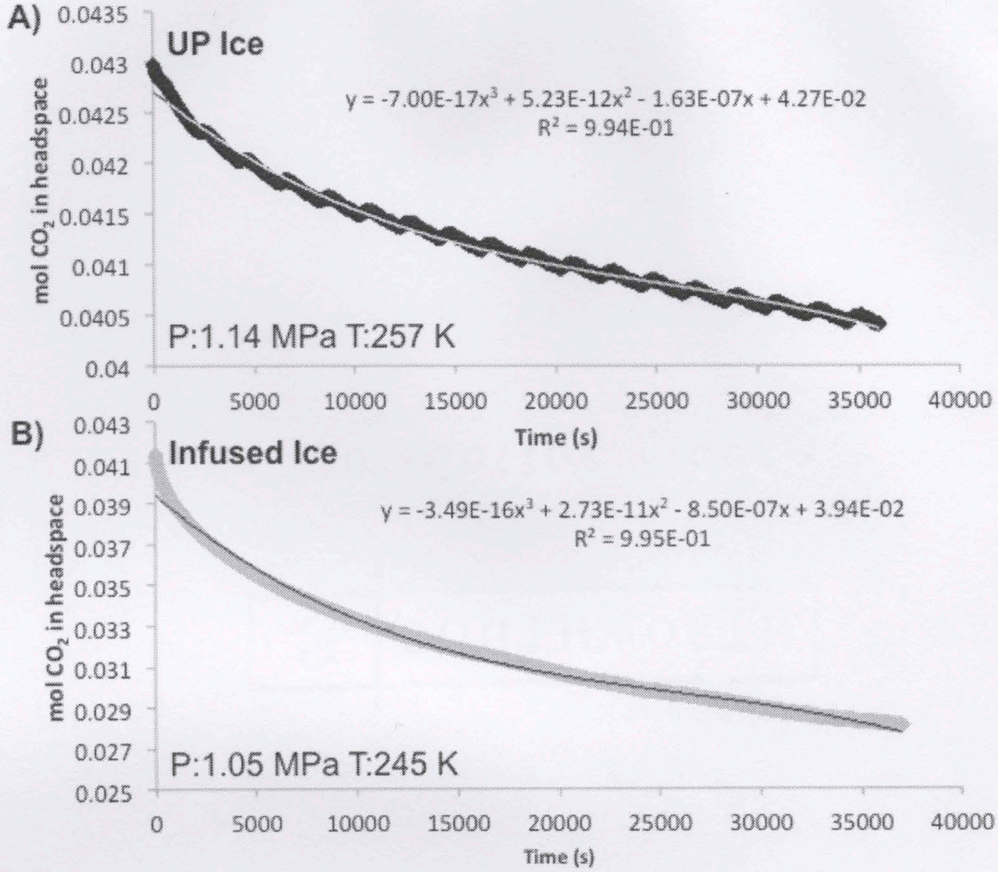

Figure 9 Result of a formation experiment on UP (A) and infused (B) ice. Hydrate formation is initially rapid but slows as formation becomes controlled by diffusion. These formation experiments were at similar pressure conditions but the infused experiments showed significantly more hydrate formation, 0.013 mol versus 0.0025 mol in UP water ice.

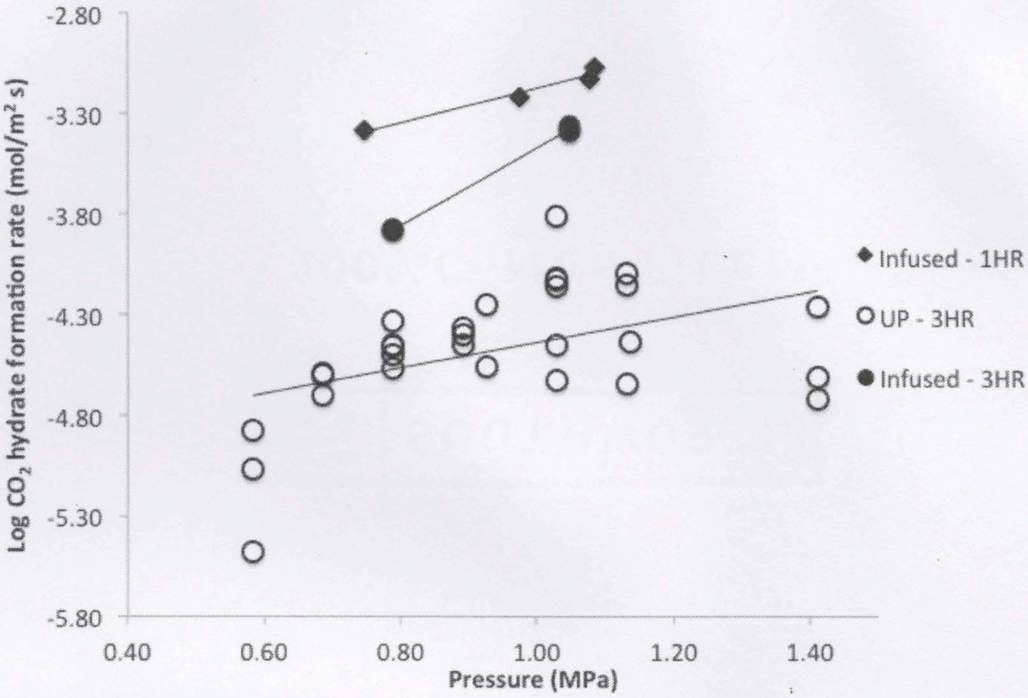

Figure 10 Increasing pressure increases the initial rate of hydrate formation. At isobaric conditions, infusion of CO_2 into the starting ice also increased the formation rate by a half order of magnitude.

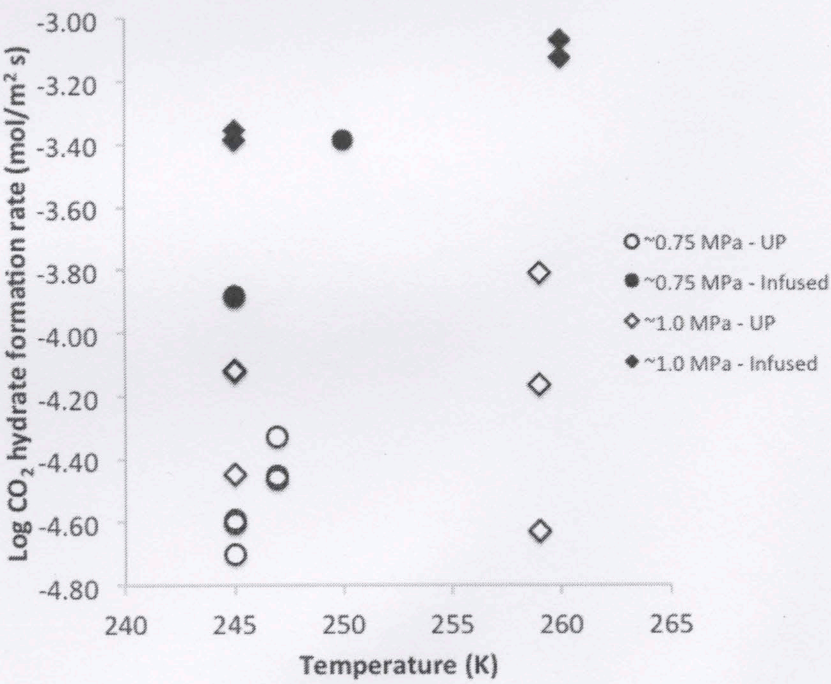

Figure 11 The influence of pressure, temperature and CO_2 infusion on CO_2 hydrate formation rates. Hydrates form faster at higher pressures and temperatures, however the

effect of gas bubbles trapped in the ice has a significant effect. The presence of trapped CO_2 bubble increased intial formation rates by a half order of magnitude.

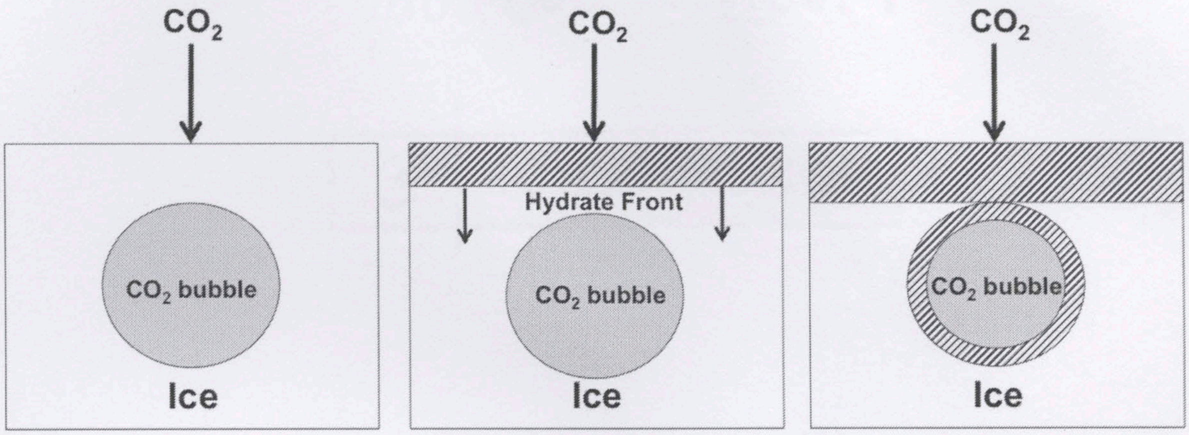

Figure 12 As the hydrate front moves downward in the infused ice experiments, it encounters the CO_2 filled bubbles. These bubbles not only provide a larger surface area for hydrate formation, but also more material (CO_2) for clathration.

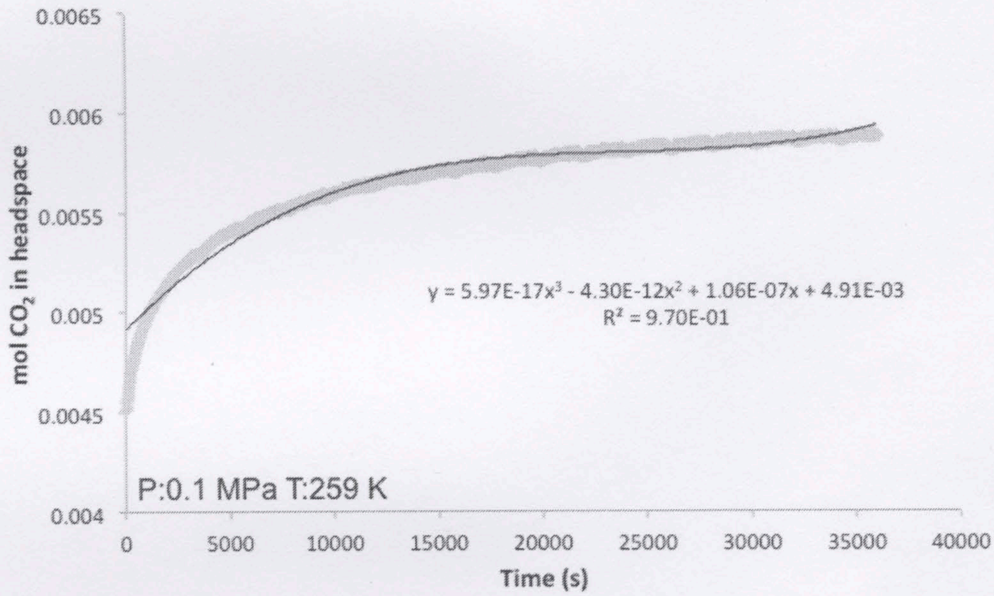

Figure 13 During dissociation experiments, the increase in headspace gas was monitored. As the curve levels off, the dissociation nears completion.

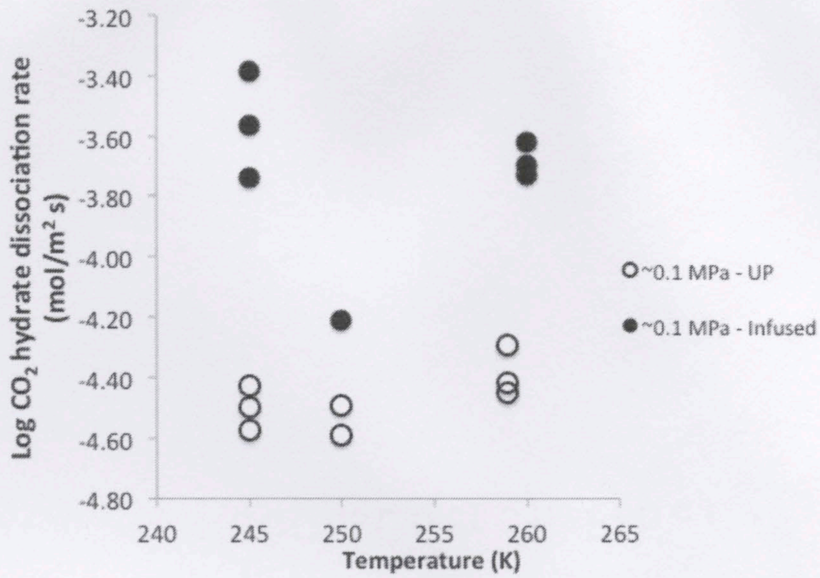

Figure 14 CO_2 hydrate dissociation rates are highly dependent on temperature due to the effects of anomalous self-preservation noted in other studies (Stern et al., 2003; Kuhs et al., 2004; Falenty and Kuhs, 2009). The infused ice experiments also dissociated faster than the UP ice, likely due to higher concentrations of clathrate in the experiments due to faster formation rates.

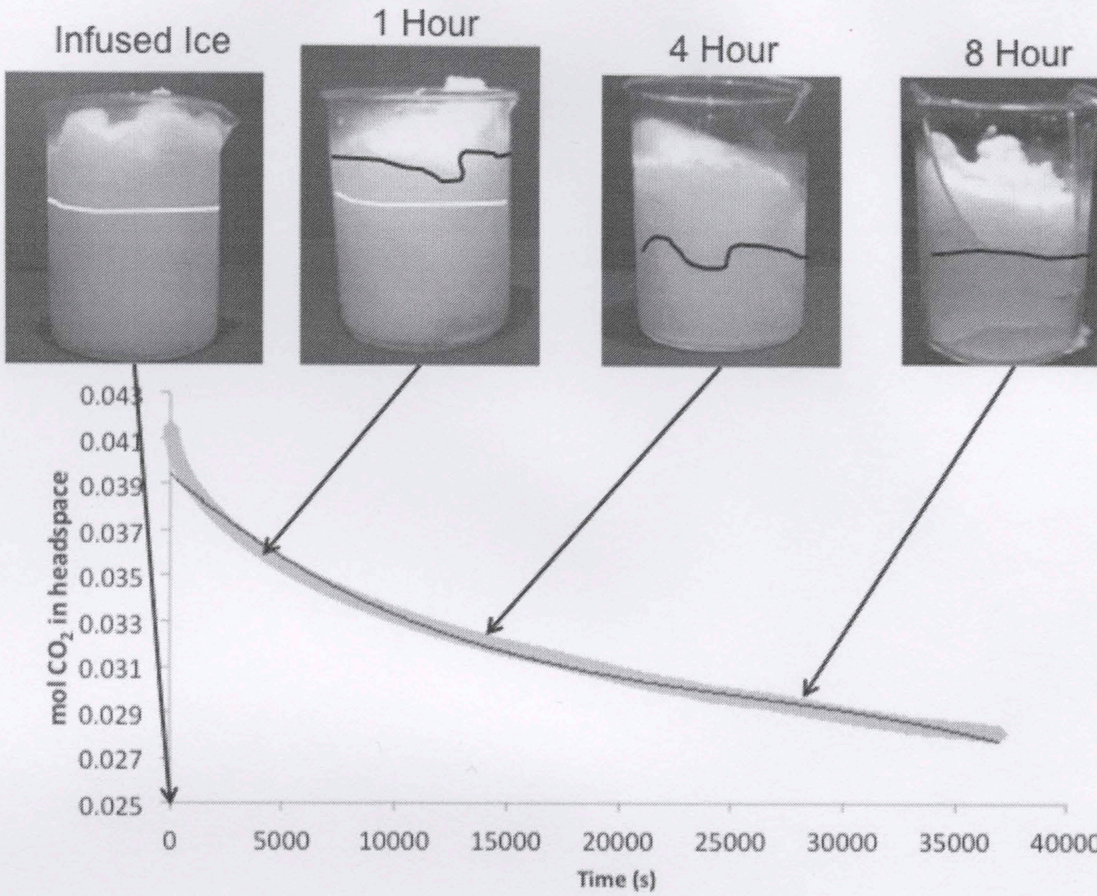

Figure 15 The time lapse photos show the rate of hydrate formation. The photos show the growth on infused ice (base of banding represented by the white line). Most of the hydrate (black line) was formed by 4 hours. This is likely when diffusion takes over as the rate controlling mechanism as proposed by Wang et al. (2002), Kuhs et al. (2006) and Gainey and Elwood Madden (2012).

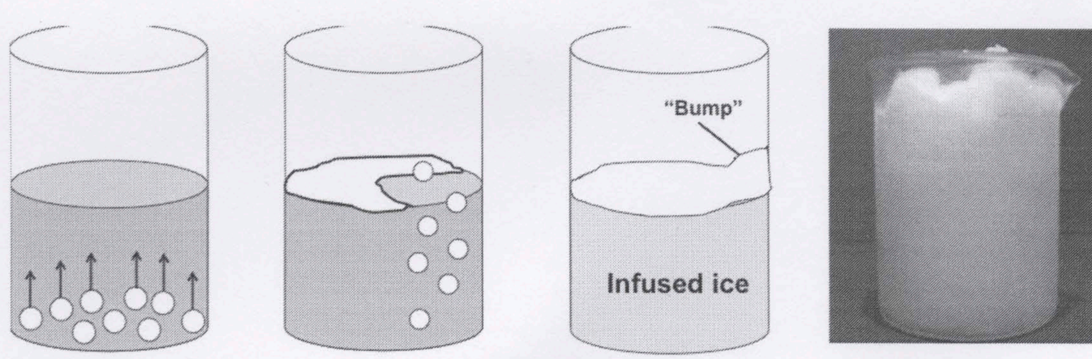

Figure 16 As the water freezes (dark gray), CO_2 (white bubbles) is exsolved and rises to the top. As the water freezes at the top the gas has a smaller area to escape. Eventually the bubbling water freezes over forming the bump.

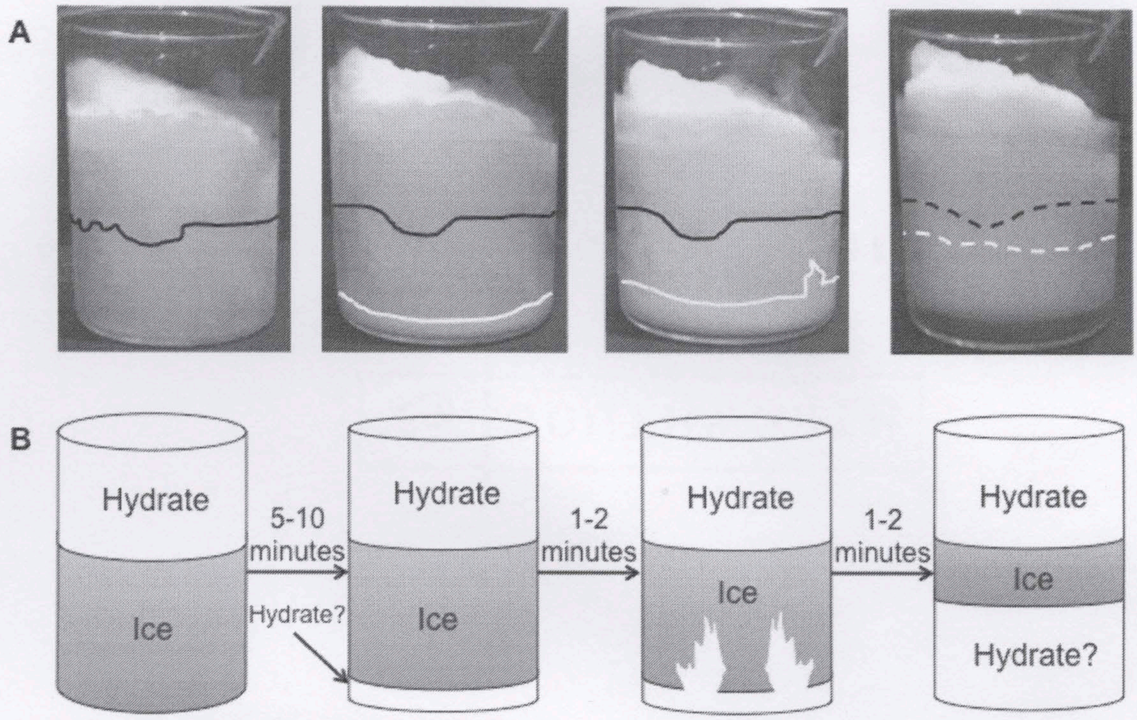

Figure 17 A) Photos of the unusual dissociation during warming B) Cartoon of the same process. Observing the hydrate formed on the CO_2 infused ice initially revealed an opaque layer of hydrate (black line) over a semitransparent ice. After 5-10 minutes a new layer of hydrate appeared to form at the bottom of the ice (white line). The hydrate layer then appears to move away from the main source of heat (counter top) toward the coldest part of the ice. After 10-15 minutes the original hydrate and new hydrate are nearly indistinguishable (dashed black and white lines).

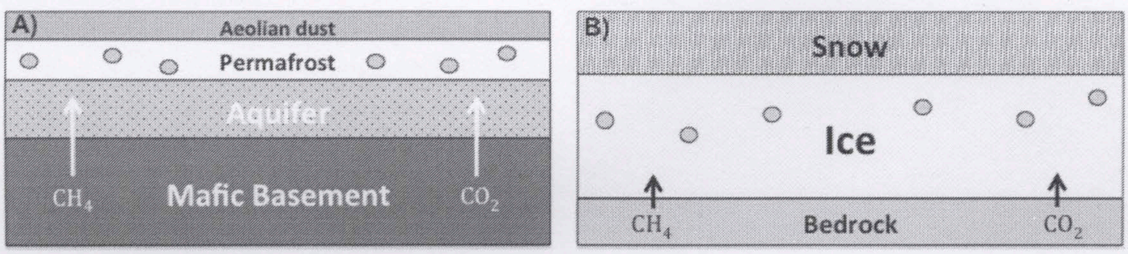

Figure 18 Gas advecting from subsurface on Mars will encounter trapped gas bubbles either in permafrost (A) or polar ice caps (B). These bubbles provide surface area and more reactants to form hydrates.

References

Archer, D., 2005, Fate of fossil fuel CO2 in geologic time: JOURNAL OF GEOPHYSICAL RESEARCH-OCEANS, v. 110, no. C9.

Bender, M., Sowers, T., and Lipenkov, V., 1995, On the concentrations of O2, N2, and Ar in trapped gases from ice cores: Journal of Geophysical Research: Atmospheres, v. 100, no. D9, p. 18651–18660, doi: 10.1029/94JD02212.

Bereiter, B., Schwander, J., Lüthi, D., and Stocker, T.F., 2009, Change in CO2 concentration and O2/N2 ratio in ice cores due to molecular diffusion: Geophysical Research Letters, v. 36, no. 5, p. n/a–n/a, doi: 10.1029/2008GL036737.

Bishnoi, P.R., and Natarajan, V., 1996, Formation and decomposition of gas hydrates: Fluid Phase Equilibria, v. 117, no. 1–2, p. 168–177, doi: 10.1016/0378-3812(95)02950-8.

Brewer, P.G., Peltzer, E.T., Friederich, G., Aya, I., and Yamane, K., 2000, Experiments on the ocean sequestration of fossil fuel CO2: pH measurements and hydrate formation: Marine Chemistry, v. 72, no. 2–4, p. 83–93, doi: 10.1016/S0304-4203(00)00074-8.

Calmels, F., and Allard, M., 2004, Ice segregation and gas distribution in permafrost using tomodensitometric analysis: Permafrost and Periglacial Processes, v. 15, no. 4, p. 367–378, doi: 10.1002/ppp.508.

Chassefière, E., Dartois, E., Herri, J.-M., Tian, F., Schmidt, F., Mousis, O., and Lakhlifi, A., 2013, CO2–SO2 clathrate hydrate formation on early Mars: Icarus, v. 223, no. 2, p. 878–891, doi: 10.1016/j.icarus.2013.01.001.

Chastain, B.K., and Chevrier, V., 2007, Methane clathrate hydrates as a potential source for martian atmospheric methane: Planetary and Space Science, v. 55, no. 10, p. 1246–1256, doi: 10.1016/j.pss.2007.02.003.

Circone, S., Stern, L.A., Kirby, S.H., Durham, W.B., Chakoumakos, B.C., Rawn, C.J., Rondinone, A.J., and Ishii, Y., 2003, CO2 Hydrate: Synthesis, Composition, Structure, Dissociation Behavior, and a Comparison to Structure I CH4 Hydrate: The Journal of Physical Chemistry B, v. 107, no. 23, p. 5529–5539, doi: 10.1021/jp027391j.

Cramer, W., Bondeau, A., Woodward, F.I., Prentice, I.C., Betts, R.A., Brovkin, V., Cox, P.M., Fisher, V., Foley, J.A., Friend, A.D., Kucharik, C., Lomas, M.R., Ramankutty, N., Sitch, S., et al., 2001, Global response of terrestrial ecosystem structure and function to CO2 and climate change: results from six dynamic global vegetation models: Global Change Biology, v. 7, no. 4, p. 357–373, doi: 10.1046/j.1365-2486.2001.00383.x.

Dallimore, S.R., and Collett, T.S., 1995, Intrapermafrost gas hydrates from a deep core hole in the Mackenzie Delta, Northwest Territories, Canada: Geology, v. 23, no. 6, p. 527–530, doi: 10.1130/0091-7613(1995)023<0527:IGHFAD>2.3.CO;2.

Falenty, A., and Kuhs, W.F., 2009, "Self-Preservation" of CO2 Gas Hydrates—Surface Microstructure and Ice Perfection: The Journal of Physical Chemistry B, v. 113, no. 49, p. 15975–15988, doi: 10.1021/jp906859a.

Falenty, A., Salamatin, A.N., and Kuhs, W.F., 2013, Kinetics of CO2-Hydrate Formation from Ice Powders: Data Summary and Modeling Extended to Low Temperatures: The Journal of Physical Chemistry C, v. 117, no. 16, p. 8443–8457, doi: 10.1021/jp310972b.

Feldman, W.C., Prettyman, T.H., Maurice, S., Plaut, J.J., Bish, D.L., Vaniman, D.T., Mellon, M.T., Metzger, A.E., Squyres, S.W., Karunatillake, S., Boynton, W.V., Elphic, R.C., Funsten, H.O., Lawrence, D.J., et al., 2004, Global distribution of near-surface hydrogen on Mars: Journal of Geophysical Research: Planets, v. 109, no. E9, p. n/a–n/a, doi: 10.1029/2003JE002160.

Fuller, R.C., Prevost, J.H., and Piri, M., 2006, Three-phase equilibrium and partitioning calculations for CO2 sequestration in saline aquifers: Journal of Geophysical Research: Solid Earth, v. 111, no. B6, p. n/a–n/a, doi: 10.1029/2005JB003618.

Gainey, S.R., and Elwood Madden, M.E., 2012, Kinetics of methane clathrate formation and dissociation under Mars relevant conditions: Icarus, v. 218, no. 1, p. 513–524, doi: 10.1016/j.icarus.2011.12.019.

Goel, N., 2006, In situ methane hydrate dissociation with carbon dioxide sequestration: Current knowledge and issues: Journal of Petroleum Science and Engineering, v. 51, no. 3–4, p. 169–184, doi: 10.1016/j.petrol.2006.01.005.

Hester, K.C., and Brewer, P.G., 2009, Clathrate Hydrates in Nature: Annual Review of Marine Science, v. 1, no. 1, p. 303–327, doi: 10.1146/annurev.marine.010908.163824.

Hoffman, N., 2000, White Mars: A New Model for Mars' Surface and Atmosphere Based on CO2: Icarus, v. 146, no. 2, p. 326–342, doi: 10.1006/icar.2000.6398.

Jeffries, M.O., Morris, K., Weeks, W.F., and Wakabayashi, H., 1994, Structural and stratigraphie features and ERS 1 synthetic aperture radar backscatter characteristics of ice growing on shallow lakes in NW Alaska, winter 1991–1992: Journal of Geophysical Research: Oceans, v. 99, no. C11, p. 22459–22471, doi: 10.1029/94JC01479.

Kawamura, T., Komai, T., Yamamoto, Y., Nagashima, K., Ohga, K., and Higuchi, K., 2002, Growth kinetics of CO2 hydrate just below melting point of ice: Journal of Crystal Growth, v. 234, no. 1, p. 220–226, doi: 10.1016/S0022-0248(01)01639-6.

Kieffer, H.H., Christensen, P.R., Martin, T.Z., Miner, E.D., and Palluconi, F.D., 1976, Temperatures of the Martian Surface and Atmosphere: Viking Observation of Diurnal and Geometric Variations: Science, v. 194, no. 4271, p. 1346–1351, doi: 10.1126/science.194.4271.1346.

Kipfstuhl, S., Pauer, F., Kuhs, W.F., and Shoji, H., 2001, Air bubbles and Clathrate hydrates in the transition zone of the NGRIP Deep Ice Core: Geophysical Research Letters, v. 28, no. 4, p. 591–594, doi: 10.1029/1999GL006094.

Koh, C.A., 2002, Towards a fundamental understanding of natural gas hydrates: Chemical Society Reviews, v. 31, no. 3, p. 157–167, doi: 10.1039/b008672j.

Kuhs, W.F., Genov, G., Staykova, D.K., and Hansen, T., 2004, Ice perfection and onset of anomalous preservation of gas hydrates: Physical Chemistry Chemical Physics, v. 6, no. 21, p. 4917–4920, doi: 10.1039/B412866D.

Kuhs, W.F., Staykova, D.K., and Salamatin, A.N., 2006, Formation of Methane Hydrate from Polydisperse Ice Powders: J. Phys. Chem. B, v. 110, no. 26, p. 13283–13295, doi: 10.1021/jp061060f.

Lashof, D.A., and Ahuja, D.R., 1990, Relative contributions of greenhouse gas emissions to global warming: Nature, v. 344, no. 6266, p. 529–531, doi: 10.1038/344529a0.

Leeman, J.R., and Elwood Madden, M.E., 2010, CO_2 Clathrate Formation and Dissociation Rates Below 273K.

Lipenkov, V.Y., 2000, Air bubbles and air-hydrate crystals in the Vostok ice core: Physics of Ice Core Records,, p. 327–358.

Liu, X., and Flemings, P.B., 2006, Passing gas through the hydrate stability zone at southern Hydrate Ridge, offshore Oregon: Earth and Planetary Science Letters, v. 241, no. 1–2, p. 211–226, doi: 10.1016/j.epsl.2005.10.026.

McCallum, S.D., Riestenberg, D.E., Zatsepina, O.Y., and Phelps, T.J., 2007, Effect of pressure vessel size on the formation of gas hydrates: Journal of Petroleum Science and Engineering, v. 56, no. 1–3, p. 54–64, doi: 10.1016/j.petrol.2005.08.004.

Mienert, J., Vanneste, M., Bünz, S., Andreassen, K., Haflidason, H., and Sejrup, H.P., 2005, Ocean warming and gas hydrate stability on the mid-Norwegian margin at the Storegga Slide: Marine and Petroleum Geology, v. 22, no. 1–2, p. 233–244, doi: 10.1016/j.marpetgeo.2004.10.018.

Milkov, A.V., 2005, Molecular and stable isotope compositions of natural gas hydrates: A revised global dataset and basic interpretations in the context of geological settings: Organic Geochemistry, v. 36, no. 5, p. 681–702, doi: 10.1016/j.orggeochem.2005.01.010.

Miller, S.L., 1969, Clathrate hydrates of air in antarctic ice: Science (New York, N.Y.), v. 165, no. 3892, p. 489–490, doi: 10.1126/science.165.3892.489.

Miller, S.L., and Smythe, W.D., 1970, Carbon Dioxide Clathrate in the Martian Ice Cap: Science, v. 170, no. 3957, p. 531–533, doi: 10.1126/science.170.3957.531.

Ohmura, R., Ogawa, M., Yasuoka, K., and Mori, Y.H., 2003, Statistical Study of Clathrate-Hydrate Nucleation in a Water/Hydrochlorofluorocarbon System: Search for the Nature of the "Memory Effect:" The Journal of Physical Chemistry B, v. 107, no. 22, p. 5289–5293, doi: 10.1021/jp027094e.

Owen, T., Biemann, K., Rushneck, D.R., Biller, J.E., Howarth, D.W., and Lafleur, A.L., 1977, The Composition of the Atmosphere at the Surface of Mars: Journal of Geophysical Research, v. 82, no. 28, p. 4635–4639, doi: 10.1029/JS082i028p04635.

Oze, C., and Sharma, 2005, Have olivine, will gas: Serpentinization and the abiogenic production of methane on Mars: Geophysical Research Letters, v. 32, no. 10, doi: 10.1029/2005GL022691.

Root, M.J., and Elwood Madden, M.E., 2012, Potential effects of obliquity change on gas hydrate stability zones on Mars: Icarus, v. 218, no. 1, p. 534–544, doi: 10.1016/j.icarus.2011.12.024.

Scholander, P.F., Hemmingsen, E.A., Coachman, L.K., and Nutt, D.C., 1961, Composition of Gas Bubbles in Greenland Icebergs: Journal of Glaciology, v. 3, no. 29, p. 813–822.

Shoji, H., and Langway, C.C., 1982, Air hydrate inclusions in fresh ice core: , Published online: 05 August 1982; | doi:10.1038/298548a0, v. 298, no. 5874, p. 548–550, doi: 10.1038/298548a0.

Sloan, E.D., 1998, Gas Hydrates: Review of Physical/Chemical Properties: Energy Fuels, v. 12, no. 2, p. 191–196, doi: 10.1021/ef970164+.

Sloan, E.D., and Koh, C., 2008, Clathrate Hydrates of Natural Gases, Third Edition: CRC Press.

Stern, L.A., Circone, S., Kirby, S.H., and Durham, W.B., 2003, Temperature, pressure, and compositional effects on anomalous or “self” preservation of gas hydrates: Canadian Journal of Physics, v. 81, no. 1-2, p. 271–283, doi: 10.1139/p03-018.

Svandal, A., Kuznetsova, T., and Kvamme, B., 2006, Thermodynamic properties and phase transitions in the H2O/CO2/CH4 system: Fluid Phase Equilibria, v. 246, no. 1–2, p. 177–184, doi: 10.1016/j.fluid.2006.06.003.

Takeya, S., Hondoh, T., and Uchida, T., 2000, In Situ Observation of CO2 Hydrate by X-ray Diffraction: Annals of the New York Academy of Sciences, v. 912, no. 1, p. 973–982, doi: 10.1111/j.1749-6632.2000.tb06852.x.

Takeya, S., Hori, A., Hondoh, T., and Uchida, T., 2000, Freezing-Memory Effect of Water on Nucleation of CO2 Hydrate Crystals: The Journal of Physical Chemistry B, v. 104, no. 17, p. 4164–4168, doi: 10.1021/jp993759+.

Tegze, G., Pusztai, T., Tóth, G., Gránásy, L., Svandal, A., Buanes, T., Kuznetsova, T., and Kvamme, B., 2006, Multiscale approach to CO[sub 2] hydrate formation in aqueous solution: Phase field theory and molecular dynamics. Nucleation and growth: The Journal of Chemical Physics, v. 124, no. 23, p. 234710, doi: 10.1063/1.2207138.

Thomas, C., Mousis, O., Picaud, S., and Ballenegger, V., 2009, Variability of the methane trapping in martian subsurface clathrate hydrates: Planetary and Space Science, v. 57, no. 1, p. 42–47, doi: 10.1016/j.pss.2008.10.003.

Wang, X., Schultz, A.J., and Halpern, Y., 2002, Kinetics of Methane Hydrate Formation from Polycrystalline Deuterated Ice: The Journal of Physical Chemistry A, v. 106, no. 32, p. 7304–7309, doi: 10.1021/jp025550t.

Wiebe, R., and Gaddy, V.L., 1940, The Solubility of Carbon Dioxide in Water at Various Temperatures from 12 to 40° and at Pressures to 500 Atmospheres. Critical Phenomena*: J. Am. Chem. Soc., v. 62, no. 4, p. 815–817, doi: 10.1021/ja01861a033.